Frontiers of Optoelectronics (2024) 17:13
https://doi.org/10.1007/s12200-024-00116-4

Frontiers of Optoelectronics

RESEARCH ARTICLE

MEMS-actuated terahertz metamaterials driven by phase-transition materials

Zhixiang Huang[1] · Weipeng Wu[2] · Eric Herrmann[1] · Ke Ma[1] · Zizwe A. Chase[3] · Thomas A. Searles[3] · M. Benjamin Jungfleisch[2] · Xi Wang[1]

Received: 28 February 2024 / Accepted: 15 April 2024
© The Author(s) 2024

Abstract
The non-ionizing and penetrative characteristics of terahertz (THz) radiation have recently led to its adoption across a variety of applications. To effectively utilize THz radiation, modulators with precise control are imperative. While most recent THz modulators manipulate the amplitude, frequency, or phase of incident THz radiation, considerably less progress has been made toward THz polarization modulation. Conventional methods for polarization control suffer from high driving voltages, restricted modulation depth, and narrow band capabilities, which hinder device performance and broader applications. Consequently, an ideal THz modulator that offers high modulation depth along with ease of processing and operation is required. In this paper, we propose and realize a THz metamaterial comprised of microelectromechanical systems (MEMS) actuated by the phase-transition material vanadium dioxide (VO_2). Simulation and experimental results of the three-dimensional metamaterials show that by leveraging the unique phase-transition attributes of VO_2, our THz polarization modulator offers notable advancements over existing designs, including broad operation spectrum, high modulation depth, ease of fabrication, ease of operation condition, and continuous modulation capabilities. These enhanced features make the system a viable candidate for a range of THz applications, including telecommunications, imaging, and radar systems.

Keywords Metamaterials · MEMS · THz · VO_2 · Phase-transition material

1 Introduction

Terahertz (THz) radiation, with frequencies ranging from 0.3 to 3×10^{12} Hz [1], bridges the gap between the microwave and infrared spectral ranges and can interact with many dielectric materials [2] and intrinsic semiconductors [3], but undergoes large absorption in liquid water [4]. THz technology has been utilized across a diverse range of applications such as imaging [5, 6], security [6], telecommunications [7], and biosensing [8], largely due to its non-ionizing [9] and penetrative characteristics. The effective application of THz radiation requires precise control and manipulation, typically facilitated by THz modulators.

Recently, significant effort has been dedicated to realizing THz modulators, leading to four primary modulation techniques [10]. Carrier concentration modulation employs gating methods or optical pumping to alter an active layer's optical conductivity, tuning the device's responsivity to THz waves. These devices have shown outstanding performance in modulation speed and amplitude modulation depth [11–13], but typically involve high gating voltages [12, 14–16]. Liquid crystal modulation utilizes the inherent birefringence of liquid crystals [17–19], but the trade-off between the thickness of the liquid crystal layer and the modulation speed impedes its further development [20, 21]. The phase-transition material vanadium dioxide (VO_2) introduces a unique THz modulation approach due to its temperature-induced insulator-to-metal transition at around 68°C [22–27]. Metasurfaces integrated with VO_2 thin films

✉ Xi Wang
wangxi@udel.edu

[1] Department of Materials Science and Engineering, College of Engineering, University of Delaware, Newark, DE 19716, USA

[2] Department of Physics and Astronomy, College of Arts and Sciences, University of Delaware, Newark, DE 19716, USA

[3] Department of Electrical and Computer Engineering, College of Engineering, University of Illinois Chicago, Chicago, IL 60607, USA

Published online: 27 May 2024

can achieve a large modulation depth with a low operation voltage. However, while conventional VO_2 devices leverage the optical properties of VO_2 before and after its phase transition, their design flexibility can be further improved by introducing geometric changes [26, 28–33]. Lastly, microelectromechanical systems (MEMS) can be designed to precisely interact with incident THz waves for effective modulation and tailorable scattered fields [21, 34–40]. Furthermore, the large geometric deformation associated with MEMS enables relatively large modulation by deforming in and out of resonance with the impinging THz wavefront. Even with these advantages, many MEMS are operated by electrostatic forces with operation voltages as high as 300 V, limiting the maximum achievable deformation and resulting modulation depth [41–44].

Typical THz modulators manipulate key parameters of incident light, such as amplitude, frequency, phase, and polarization. Among them, THz pulses with modulated polarization are promising for probing and manipulating materials via crystal lattice vibrations [45], molecular rotation and alignment [46], and spin processing [47–49]. Other key technologies that demand meticulous polarization control include THz telecommunication [50], circular dichroism spectroscopy [51], and THz coherent control of matter [52]. However, despite the recent advances in the field of polarization modulation, there are still some limitations that impede further improvement and broader applications. Many active polarization management systems demand intricate optical stimulus configurations and extended propagation lengths to detect chirality in natural substances, which result in complicated device production [53]. Traditional polarization control techniques are typically restricted in bandwidth and frequency, which exhibit suboptimal efficiency and a restricted modulation depth [19, 20, 54, 55]. Additionally, conventional methods for polarization control require high driving voltages [43], ion-gel control [51], or a sealed gas chamber [39].

Here, we propose a MEMS-based THz polarization modulator that relies on the mechanical deformation driven by the phase transition of VO_2. Our modulator, fabricated by one-step photolithography, can achieve active tuning of the polarization of THz waves with ease of operation near room temperature. The operation wavelength range and modulation depth of polarization are comparable with previous reports using high driving voltages [43] and pneumatic forces [39].

2 Results

2.1 Dynamically tunable metamaterials

We employ a tunable chiral metasurface to dynamically modulate the polarization of incident THz waves. The metasurface consists of a square lattice of patterned unit cells, with each unit built from eight spiral cantilever arms extending from the center anchor, as shown in Fig. 1a. The constant speed spiral cantilevers are equally spaced at any given angle, and the radial distance from the center of the spiral increases linearly with the angle. The spiral cantilevers are connected to a round center anchor, which is stationary during the actuation. By manipulating the length and curvature of helical structures within 3D meta-atoms, significant circular dichroism (CD) can be realized and customized for various wavelengths. Similar structures have been used to modulate the chirality of infrared light [56, 57] and microwave [58].

Tunable polarization modulation can be achieved by changing the curvature of spiral cantilevers. The polarization modulation performance is evaluated by two key parameters: the polarization azimuth rotation angle θ and the ellipticity angle η. The polarization azimuth rotation angle describes the relative rotation of the maximum polarization, while the ellipticity angle describes the shape of the polarization ellipse.

The polarization modulation performance of the proposed design in Fig. 1a was simulated using COMSOL Multiphysics as detailed in Supplementary Information. Because substrates in real devices limit the downward bending of cantilevers, we simulated two groups of spiral cantilevers, one with clockwise (CW) spiral cantilevers and the other with counterclockwise (CCW) spiral cantilevers, both approximated as perfect electrical conductors. Our device operates on a principle analogous to that of enantiomers, incorporating spiral cantilever arms to create a chiral metamaterial structure. By changing the curvature of the cantilever arms, they exhibit significant optical activity through the exploitation of first-order spatial dispersion effects. This phenomenon arises from the non-local nature of light-matter interactions, where achieving a pronounced three-dimensional spatial variation within the chiral structures is crucial for amplifying optical activity [59]. For example, when the curvature is zero and spiral cantilevers are flat, the entire unit cell is orthogonal to the THz transmission direction and only alters the polarization and ellipticity of the incident THz by a very small value, as shown in Fig. 1b and d. When the spiral cantilevers bend toward the direction of the incident THz beam and form a 3D structure at certain resonance frequencies, this position-dependent arrival time causes a rotation in the polarization azimuth angle, altering the direction of the electric field vector of the transmitted THz beam. As a result, the angle at which the electric field oscillates relative to the initial polarization direction changes, leading to a rotation in the polarization azimuth angle as in Fig. 1c and ellipticity angle as in Fig. 1e.

After validation of the design by simulations, we fabricated the device and utilized VO_2 as the activation material

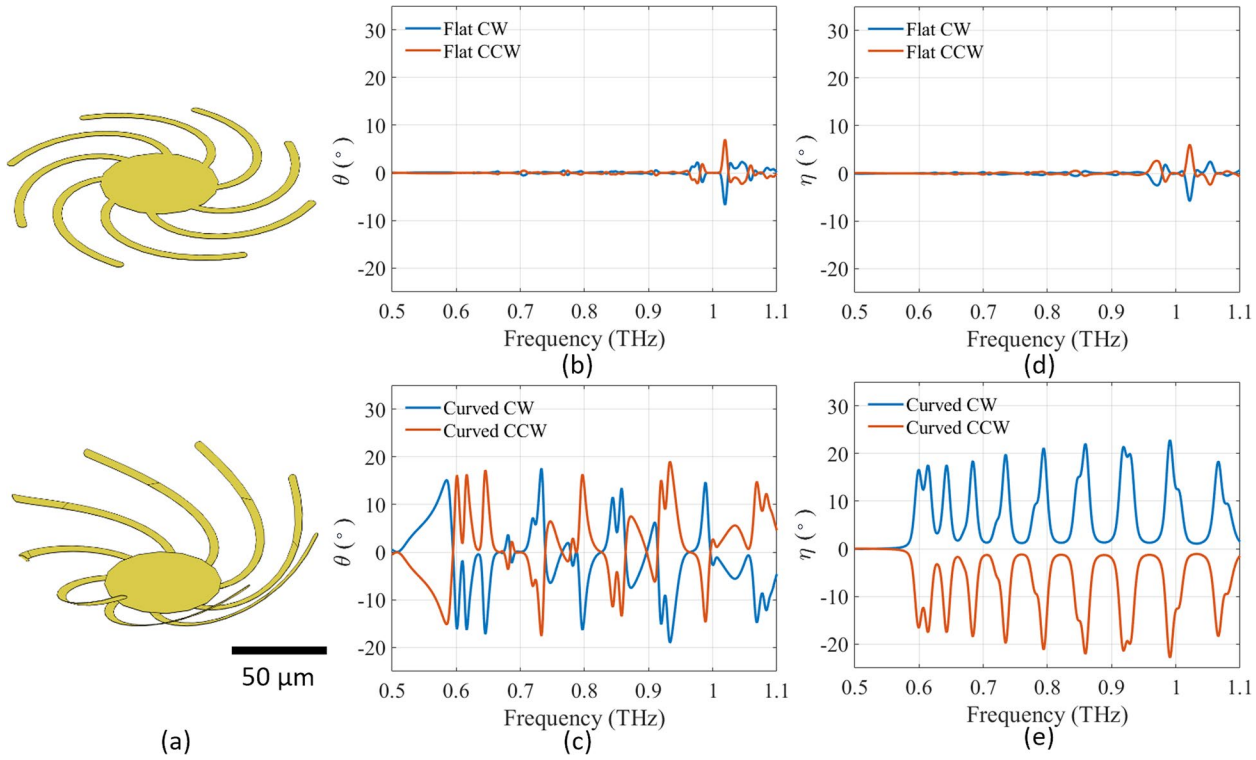

Fig. 1 **a** Schematic of counterclockwise spiral cantilevers fully flat (top) and curving up (bottom) (Note: clockwise spiral cantilevers are also made). **b** Simulated azimuth polarization rotation angle θ for flat spiral cantilevers. **c** Simulated azimuth polarization rotation angle θ for curved spiral cantilevers. **d** Simulated ellipticity angle η for flat spiral cantilevers. **e** Simulated ellipticity angle η for curved spiral cantilevers

without the requirement of a critical operating environment, e.g., either a high operation temperature or a sealed chamber as demonstrated before [39]. As a phase transition material, VO_2 is notable for its temperature-sensitive electronic and optical properties. VO_2 undergoes a 0.3% volume shrinkage during its phase transition, making it an excellent actuation material with a high volumetric working density [25]. In comparison with other materials such as thermal expansion substances [60, 61], piezoelectrics [62, 63], and shape memory alloys [64, 65], VO_2-based actuators demonstrate superior performance. While their volumetric working densities reach up to 7 J/cm^3, they exhibit a rapid response time in the picosecond range for the insulator-to-metal phase-transition and up to 6 kHz for cycling [66–68].

To integrate VO_2 as the actuation material, we employed a three-layer (gold-chromium-VO_2) cantilever design, which provides high design flexibility and arbitrary control of curvatures [27] as shown in Fig. 2a inset. The curvature of a cantilever is determined by the combined residual stresses during the fabrication process in all three layers. When VO_2 undergoes a phase transition, the volume shrinkage alters the internal stresses and leads to a change in the curvature of the cantilever.

To design the three-layer cantilever, we adapted the model by Nikishkov (Eqs. (1) – (3)) to calculate the curvature change before and after the VO_2 phase transition [27, 69]. The curvature (K) of a cantilever is given by

$$K = \frac{3\sum_{n=1}^{m} E_n' t_n (y_n + y_{n-1} - 2y_b)(c - (1+\nu_n)\varepsilon_n)}{2\sum_{n=1}^{m} E_n' t_n \left[y_n^2 + y_n y_{n-1} + y_{n-1}^2 - 3y_b (y_n + y_{n-1} - y_b)\right]}, \quad (1)$$

$$y_b = \frac{\sum_{n=1}^{m} E_n' t_n (y_n + y_{n-1})}{2\sum_{n=1}^{m} E_n' t_n}, \quad (2)$$

$$c = \frac{\sum_{n=1}^{m} E_n' t_n (1+\nu_n)\varepsilon_n}{\sum_{n=1}^{m} E_n' t_n}, \quad (3)$$

where E_n, ν_n, t_n, and ε_n are Young's modulus, Poisson's ratio, film thickness, and initial strain for the nth layer, respectively. And $E_n' = \frac{E_n}{(1-\nu_n^2)}$, $y_n = y_{n-1} + t_n$ and $y_0 = 0$. The Young's modulus and Poisson's ratio of the materials are available in Refs. [70, 71]. We first fabricated bi-layer cantilevers and measured their curvatures to verify the working principles and all the mechanical properties of the Au, Cr, and VO_2 thin films that are required in the calculation [72]. With all these parameters, the curvature of a cantilever before and after the phase transition of VO_2 could be predicted precisely. Using Eqs. (1) – (3), we find that the cantilever curvature is inversely proportional to the overall thickness for a fixed Au/Cr/VO_2 thickness ratio, as shown in

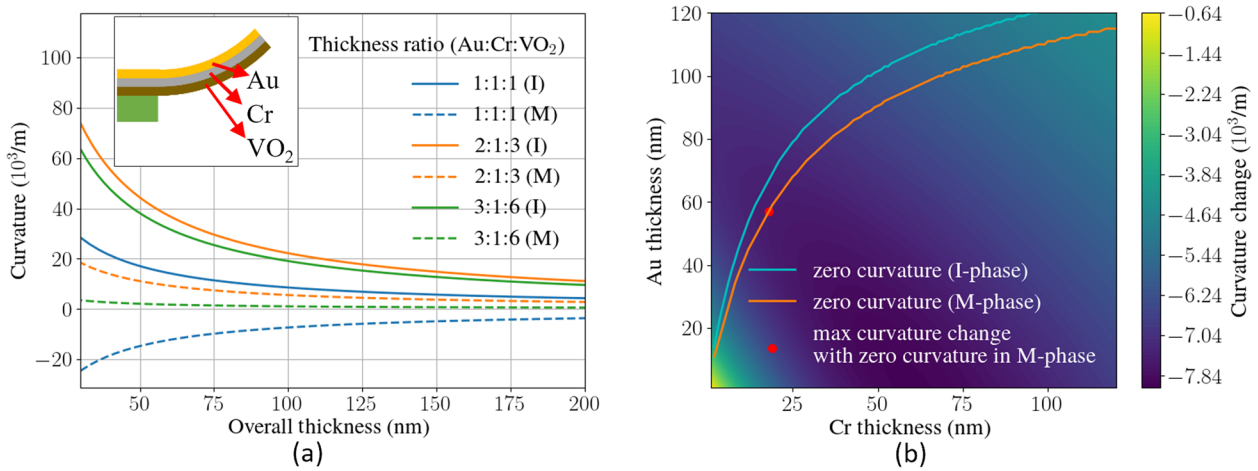

Fig. 2 **a** Cantilever curvature vs. overall thickness for different Au/Cr/VO_2 ratios. (I) and (M) indicate the VO_2 in the insulating or metallic phases. Inset: Schematic of the tri-layer cantilever and the thin film materials of the cantilevers. **b** Cantilever curvature change during actuation for different Au/Cr thicknesses and 120 nm VO_2. A deeper color indicates a larger curvature change against the VO_2 phase transition. The blue line indicates 0 curvature when VO_2 is in the insulating phase at 30 °C. The yellow line indicates 0 curvature when VO_2 is in the metallic phase at 90 °C

Fig. 2a. However, because our deposited VO_2 thin films are polycrystalline, a thinner layer leads to a lower yield in fabrication. We find that using a 120 nm thick VO_2 film could reach a balance between curvature change performance and engineering capability. Therefore, our design target is to maximize the curvature change while realizing zero curvature with metallic phase VO_2.

Figure 2b shows the curvature change values before and after the phase transition of VO_2 in cantilevers with a 120 nm thick VO_2 layer and varying thicknesses of Au/Cr thin films. The blue and yellow lines indicate where zero curvature is realized with the insulating and metallic phases of VO_2, respectively. The red dot on the yellow line corresponds to a layer thickness combination of 57 nm Au, 18 nm Cr, and 120 nm VO_2, which provides the largest curvature change against the VO_2 phase transition while maintaining zero curvature when VO_2 is in the metallic phase. Therefore, this combination is used for device fabrication.

2.2 Fabrication

The metamaterial was fabricated on a 650 μm thick double-side polished sapphire wafer. Atop the wafer, a SiO_2 layer with a thickness of 500 nm was deposited via plasma-enhanced chemical vapor deposition. Afterwards, the VO_2 layer was deposited using pulsed laser deposition. Photolithography with a laser writer was used to write the metamaterials pattern. The Cr and Au layers were sequentially deposited using an electron beam evaporator, followed by lift-off. The exposed VO_2 was then etched using a fluorine-based inductively coupled plasma etcher to expose the SiO_2 layer. The spiral cantilevers were then released using a 5% hydrofluoric acid wet etch, followed immediately by drying with a critical point dryer to ensure structural integrity.

Multiple characterization methods were used to verify the quality of the deposited 120 nm thick VO_2 thin films. As shown in the scanning electron microscope (SEM, Zeiss Merlin) image of Fig. 3a, the VO_2 surface consists of densely packed, uniformly sized grains with a rounded polyhedral shape. The size of the grains is consistent across the surface, with no larger agglomerations or clustering, indicating a uniform thin film deposition. The inset SEM image is the cross-sectional view of the 120 nm thick VO_2 thin film on a 500 nm SiO_2/sapphire substrate.

The resistance of the VO_2 thin film was measured as a function of temperature to verify the insulator–metal phase transition. As shown in Fig. 3b, the resistance decreases dramatically by more than three orders of magnitude when increasing the temperature from 20 °C to 90 °C, indicating a high-quality VO_2 film.

Figure 3c and d are optical microscope images of the spiral cantilever metamaterials. At room temperature, the spiral cantilever arms curve up and form a chiral structure, as shown in Fig. 3c. The inset is a tilted SEM image of the spiral cantilever unit cell. At high temperatures, the VO_2 undergoes the insulator–metal phase transition, and the spiral cantilever beams become fully flat, as in Fig. 3d.

2.3 Polarization modulation of THz optical activity

Optical activity modulation was studied using THz time-domain spectroscopy (THz-TDS), as shown in Fig. 4a. Three wire grid polarizers (WGP) are placed in the beam path.

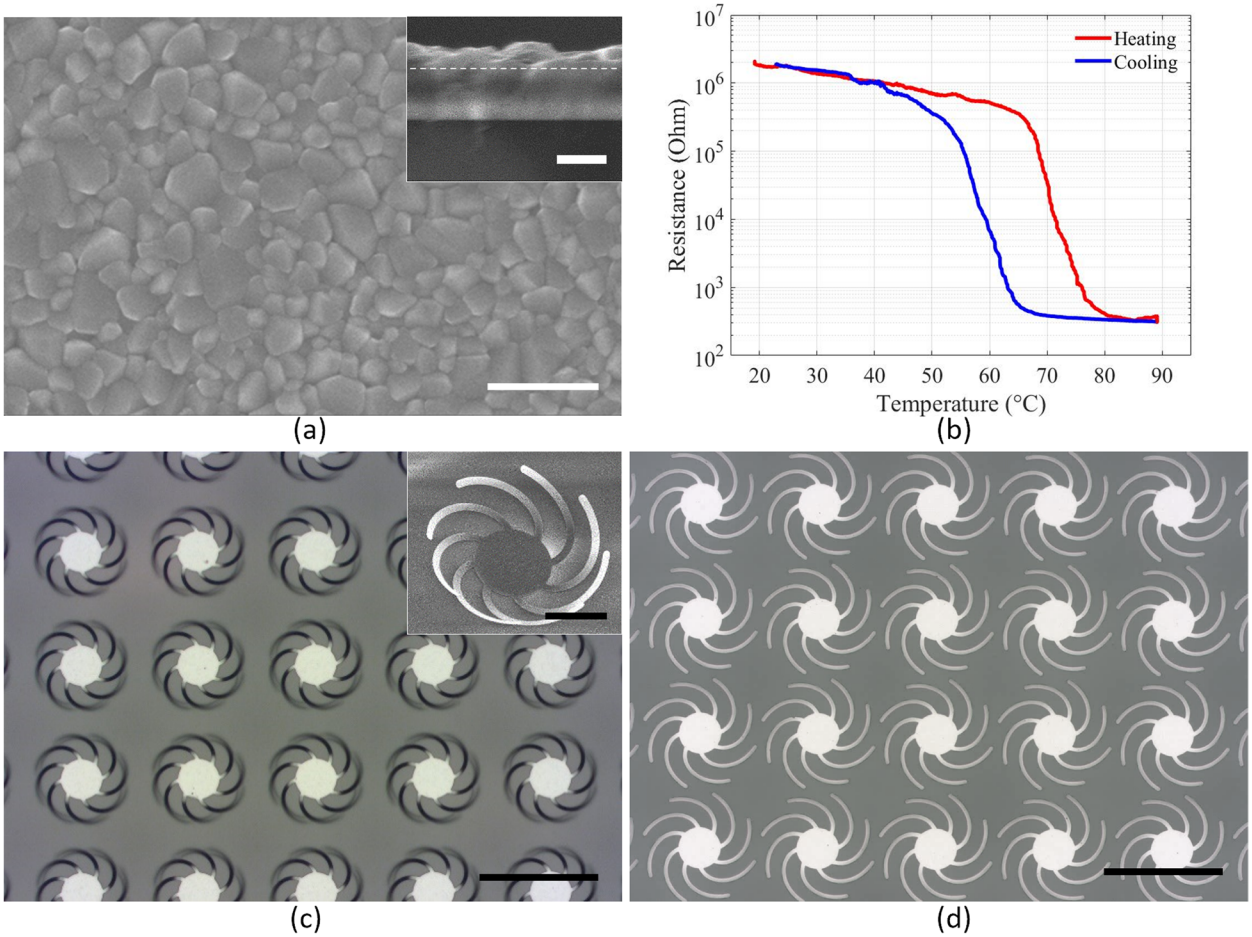

Fig. 3 **a** SEM image of the VO_2 thin film, the scale bar size is 500 nm. Inset: Cross-sectional view of ~ 120 nm VO_2 on a 500 nm SiO_2/Sapphire substrate, the dash line indicates the interface between VO_2 and SiO_2, the scale bar is 500 nm. **b** Resistance–temperature change of the VO_2 thin film. **c** Optical microscope image of the spiral cantilevers curving up at 30 °C, the scale bar is 200 µm. Inset: SEM image of the spiral cantilevers curving up. The scale bar is 50 µm. **d** Optical microscope image of the spiral cantilevers fully flat at 90 °C, the scale bar is 200 µm

WGP1 is used to linearly polarize the incident wave in the *y*-direction. To detect the change in the polarization states, another WGP3 is used as a crossed analyzer detecting the x-component of the signal to obtain the vectoral information of the arbitrary polarized THz wave, WGP2 is needed with two orientations. With this method, WGP2 extracts the polarization components of the transmitted THz wave at –45° and + 45° with the horizontal (*x*) axis ($E_1(t)$ and $E_2(t)$, respectively) [73].

By collecting the time domain data as described in the Supplementary Information, azimuth rotation angle change θ and ellipticity angle change η can be calculated [73]. The corresponding results are presented in Fig. 4b, c, and d. Figure 4b plots the θ change, and Fig. 4c plots the η change before and after the phase transition of VO_2 across a range of frequencies (0.5–1.1 THz). θ_0 and η_0 indicate the θ and η values measured at 90 °C, while θ and η indicate the values measured at other temperatures (30 °C in Fig. 4b and c). As the temperature rises from 30 °C to 90 °C, the spiral cantilever structure deforms from curved up to almost flat, and the θ values at different frequency ranges can be effectively modulated. Additionally, the ellipticity angle values indicate that the spiral cantilevers not only modified the direction of polarization but also converted the incoming linearly polarized THz waves into a partial circular polarization. In Fig. 4b and c, the error bars represent the uncertainty introduced by the potential misalignment of the three polarizers, each of which may deviate by up to ± 5° from its intended orientation. Considering these variations for all three polarizers, plots for both the polarization azimuthal rotation angle and the ellipticity angle are generated.

The mismatch between simulation and experimental results is likely from the modeling in COMSOL simulations. In COMSOL simulation, we built the structure with the same geometry as the real device but used a perfect electrical conductor (PEC) layer with zero thickness to represent the spiral cantilevers. Due to the severe scale difference between nanometer-thick layers and hundreds of micron-lengths in

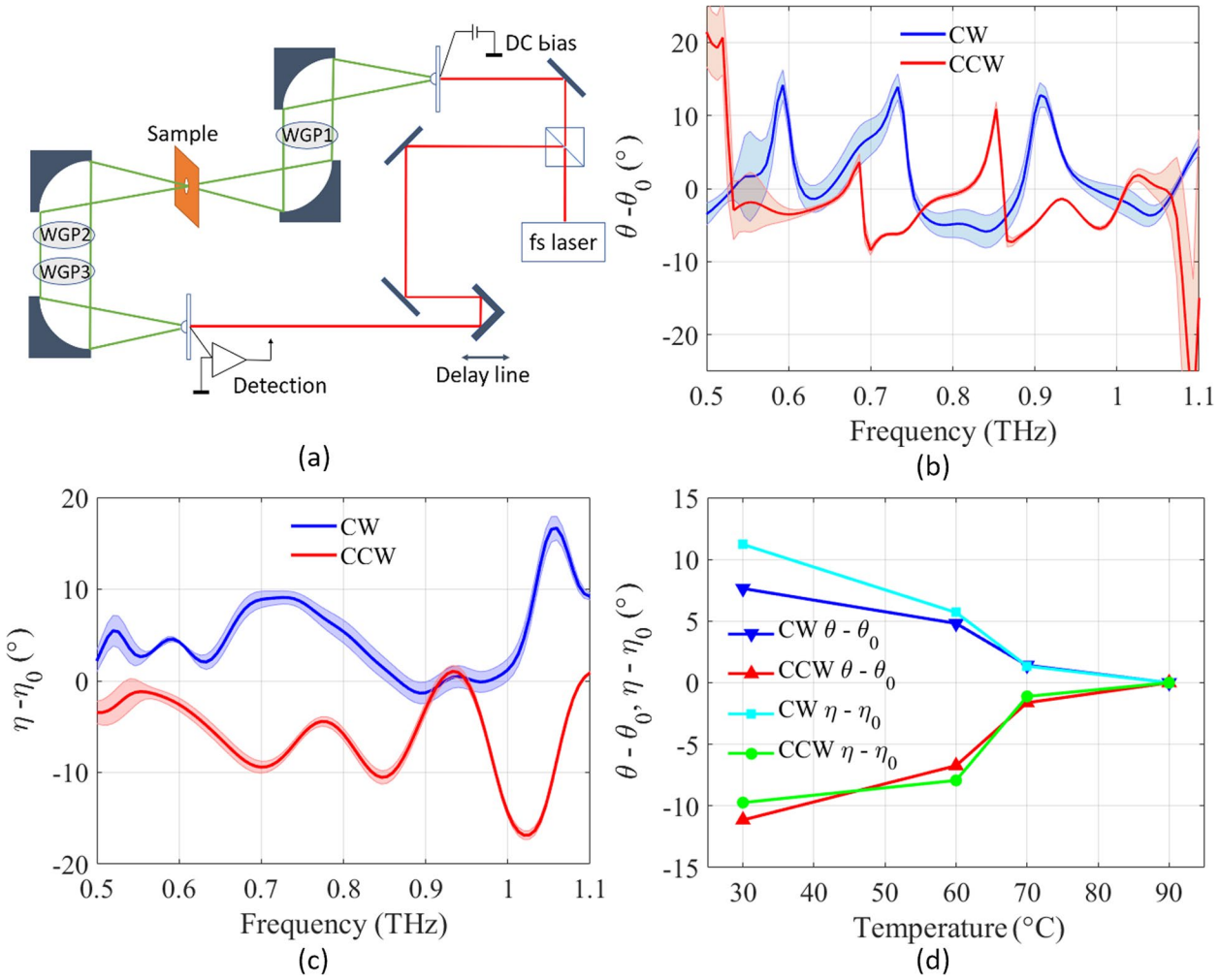

Fig. 4 **a** Schematic of the THz-TDS system. **b** Measured azimuth polarization rotation angle changes between the curved state, θ (30 °C), and the flat state θ_0 for clockwise and counterclockwise spirals. **c** Measured ellipticity angle changes between the curved state η (30 °C), and the flat state η_0, for clockwise and counterclockwise spirals. **d** Measured azimuth polarization rotation angle change θ–θ_0 and ellipticity angle change η–η_0 vs. temperature at 0.72 THz

three dimensions, implanting real devices in COMSOL simulations causes an unaffordable number of meshing elements. Therefore, we must use the PEC model to perform an approximated simulation of the modulation principles. In addition, both fabrication and characterization will introduce slight variances sample by sample. The combined effect may cause some mismatches between the simulation and experimental results, and among devices.

Figure 4d shows the variation in azimuth rotation angle at 0.72 THz as the temperature is increased. As the temperature rises from room temperature to 90 °C, the measured θ and η values decrease correspondingly. A substantial 10° shift in θ and η are observed with the temperature change. Notably, a significant shift occurs when the temperature changes from 60 °C to 70 °C across the phase-transition of VO_2, resulting in a change of more than 5° in both θ and η within only a 10 °C temperature difference. The extent of the θ and η modulations showcase the material's high sensitivity to temperature changes. This is particularly noteworthy because it underscores the capability of the metamaterial to function as a versatile modulator across a broad spectrum of operational conditions.

The comparison with previous works in THz polarization modulation is summarized in Table S1 of the Supplementary Information. The modulation of θ and η (about 15°) achieved with our device is comparable with previous reports using high driving voltages (about 6°) [43] and pneumatic forces (about 28°) [39]. While providing a reasonably large modulation depth and broad operation wavelength range, our devices are fabricated by one-step photolithography and actuated only by a small temperature increase near room temperature.

3 Conclusion

In conclusion, MEMS-actuated terahertz metamaterials for polarization modulation driven by phase-transition materials are demonstrated. By harnessing the phase-transition properties of the material VO_2, our THz metamaterials exhibit efficient and broad-spectrum THz polarization modulation with a simple operational approach. These characteristics make it a promising candidate for diverse THz applications such as telecommunication, THz imaging, and biosensing. Fabricating the spiral cantilevers onto a suspended membrane may allow the cantilevers to flex in both upward and downward directions, facilitating bidirectional tuning, which is expected to significantly enhance the versatility of our device. In addition, by integrating a heating circuit directly onto the sample, we anticipate a marked improvement in modulation speed. This will enable faster response times, making our device more efficient and suitable for a broader range of applications.

Supplementary Information The online version contains supplementary material available at https://doi.org/10.1007/s12200-024-00116-4.

Acknowledgements This research was primarily supported by NSF through the University of Delaware Materials Research Science and Engineering Center DMR-2011824.

Authors' contributions ZH and XW conceived the original idea and designed the experiment. ZH, EH, KM, ZC, and TS performed structural designs and simulations. ZH fabricated the samples. ZH, WW, and XW set up the TDTS and performed the TDTS characterizations. Z.H. analyzed the experimental data with the help of WW, EH, MBJ, and XW. ZH and XW prepared the initial manuscript. XW, MBJ, and TS co-supervised and directed the research. All authors participated in the discussion and contributed to refining the manuscript. All authors read and approved the final manuscript.

Availability of data and materials The data that support the findings of this study are available from the corresponding author, upon reasonable request.

Declarations

Competing interests The authors declare no conflict of interest.

Open Access This article is licensed under a Creative Commons Attribution 4.0 International License, which permits use, sharing, adaptation, distribution and reproduction in any medium or format, as long as you give appropriate credit to the original author(s) and the source, provide a link to the Creative Commons licence, and indicate if changes were made. The images or other third party material in this article are included in the article's Creative Commons licence, unless indicated otherwise in a credit line to the material. If material is not included in the article's Creative Commons licence and your intended use is not permitted by statutory regulation or exceeds the permitted use, you will need to obtain permission directly from the copyright holder. To view a copy of this licence, visit http://creativecommons.org/licenses/by/4.0/.

References

1. International Telecommunication Union. General Secretariat: Radio regulations; additional radio regulations, resolutions and recommendations
2. Shibuya, T., Kawase, K.: 17-Terahertz applications in tomographic imaging and material spectroscopy: a review. In: Handbook of Terahertz Technology for Imaging, Sensing and Communications. Ed D. Saeedkia. Woodhead Publishing (2013)
3. Siegel, P.H.: Terahertz technology. IEEE Trans Microw Theory Tech **50**(3), 910–928 (2002)
4. Slocum, D.M., Slingerland, E.J., Giles, R.H., Goyette, T.M.: Atmospheric absorption of terahertz radiation and water vapor continuum effects. J Quant Spectrosc Radiat Transf **127**, 49–63 (2013)
5. Yamashita, M., Kawase, K., Otani, C., Kiwa, T., Tonouchi, M.: Imaging of large-scale integrated circuits using laser-terahertz emission microscopy. Opt Express **13**(1), 115–120 (2005)
6. Federici, J.F., Schulkin, B., Huang, F., Gary, D., Barat, R., Oliveira, F., Zimdars, D.: THz imaging and sensing for security applications—explosives, weapons and drugs. Semicond Sci Technol **20**(7), S266–S280 (2005)
7. Koenig, S., Lopez-Diaz, D., Antes, J., Boes, F., Henneberger, R., Leuther, A., Tessmann, A., Schmogrow, R., Hillerkuss, D., Palmer, R., Zwick, T., Koos, C., Freude, W., Ambacher, O., Leuthold, J., Kallfass, I.: Wireless sub-THz communication system with high data rate. Nat Photonics **7**(12), 977–981 (2013)
8. Nagel, M., Först, M., Kurz, H.: THz biosensing devices: fundamentals and technology. J Phys Condens Matter **18**(18), S601–S618 (2006)
9. Zhao, L., Hao, Y.H., Peng, R.Y.: Advances in the biological effects of terahertz wave radiation. Mil Med Res **1**(1), 26 (2014)
10. Herrmann, E., Gao, H., Huang, Z., Sitaram, S.R., Ma, K., Wang, X.: Modulators for mid-infrared and terahertz light. J Appl Phys **128**(14), 140903 (2020)
11. Chen, H.T., Padilla, W.J., Zide, J.M., Gossard, A.C., Taylor, A.J., Averitt, R.D.: Active terahertz metamaterial devices. Nature **444**(7119), 597–600 (2006)
12. Shrekenhamer, D., Rout, S., Strikwerda, A.C., Bingham, C., Averitt, R.D., Sonkusale, S., Padilla, W.J.: High speed terahertz modulation from metamaterials with embedded high electron mobility transistors. Opt Express **19**(10), 9968–9975 (2011)
13. Dutta-Gupta, S., Dabidian, N., Kholmanov, I., Belkin, M.A., Shvets, G.: Electrical tuning of the polarization state of light using graphene-integrated anisotropic metasurfaces. Philos Trans Royal Soc Math Phys Eng Sci **375**(2090), 20160061 (2017)
14. Miao, Z., Wu, Q., Li, X., He, Q., Ding, K., An, Z., Zhang, Y., Zhou, L.: Widely tunable terahertz phase modulation with gate-controlled graphene metasurfaces. Phys Rev X **5**(4), 041027 (2015)
15. Ju, L., Geng, B., Horng, J., Girit, C., Martin, M., Hao, Z., Bechtel, H.A., Liang, X., Zettl, A., Shen, Y.R., Wang, F.: Graphene plasmonics for tunable terahertz metamaterials. Nat Nanotechnol **6**(10), 630–634 (2011)
16. Wu, Y., La-o-vorakiat, C., Qiu, X., Liu, J., Deorani, P., Banerjee, K., Son, J., Chen, Y., Chia, E.E.M., Yang, H.: Graphene terahertz modulators by ionic liquid gating. Adv Mater **27**(11), 1874–1879 (2015)
17. Si, G., Zhao, Y., Leong, E.S.P., Liu, Y.J.: Liquid-crystal-enabled active plasmonics: a review. Materials (Basel) **7**(2), 1296–1317 (2014)
18. Reuter, M., Vieweg, N., Fischer, B.M., Mikulicz, M., Koch, M., Garbat, K., Dąbrowski, R.: Highly birefringent, low-loss liquid crystals for terahertz applications. APL mater **1**(1), 012107 (2013)

19. Buchnev, O., Wallauer, J., Walther, M., Kaczmarek, M., Zheludev, N.I., Fedotov, V.A.: Controlling intensity and phase of terahertz radiation with an optically thin liquid crystal-loaded metamaterial. Appl Phys Lett. **103**(14), 141904 (2013)
20. Shrekenhamer, D., Chen, W.C., Padilla, W.J.: Liquid crystal tunable metamaterial absorber. Phys Rev Lett **110**(17), 177403 (2013)
21. Wang, L., Lin, X.W., Hu, W., Shao, G.H., Chen, P., Liang, L.J., Jin, B.B., Wu, P.H., Qian, H., Lu, Y.N., Liang, X., Zheng, Z.G., Lu, Y.Q.: Broadband tunable liquid crystal terahertz waveplates driven with porous graphene electrodes. Light Sci Appl **4**(2), e253 (2015)
22. Driscoll, T., Kim, H.T., Chae, B.G., Kim, B.J., Lee, Y.W., Jokerst, N.M., Palit, S., Smith, D.R., Di Ventra, M., Basov, D.N.: Memory metamaterials. Science **325**(5947), 1518–1521 (2009)
23. Yahiaoui, R., Chase, Z.A., Kyaw, C., Seabron, E., Mathews, J., Searles, T.A.: Dynamically tunable single-layer VO_2/metasurface based THz cross-polarization converter. J Phys D Appl Phys **54**(23), 235101 (2021)
24. Nouman, M.T., Hwang, J.H., Faiyaz, M., Lee, K.J., Noh, D.Y., Jang, J.H.: Vanadium dioxide based frequency tunable metasurface filters for realizing reconfigurable terahertz optical phase and polarization control. Opt Express **26**(10), 12922–12929 (2018)
25. Eyert, V.: The metal-insulator transitions of VO_2: a band theoretical approach. Ann Phys **514**(9), 650–704 (2002)
26. Hashemi, M.R.M., Yang, S.H., Wang, T., Sepúlveda, N., Jarrahi, M.: Electronically-controlled beam-steering through vanadium dioxide metasurfaces. Sci Rep **6**(1), 35439 (2016)
27. Dong, K., Lou, S., Choe, H.S., Liu, K., You, Z., Yao, J., Wu, J.: Stress compensation for arbitrary curvature control in vanadium dioxide phase transition actuators. Appl Phys Lett **109**(2), 023504 (2016)
28. Yang, Z., Ramanathan, S.: Breakthroughs in photonics 2014: phase change materials for photonics. Photonics J IEEE **7**, 1–5 (2015)
29. Chae, B., Youn, D.H., Kim, H.T., Sunglyul, M., Kang, K.: Fabrication and electrical properties of pure VO_2 phase films. J Korean Phys Soc **44**, 884–888 (2003)
30. Kawakubo, T., Nakagawa, T.: Phase transition in VO_2. J. Phys. Soc. Jpn **19**(4), 517–519 (1964)
31. Cai, H., Chen, S., Zou, C., Huang, Q., Liu, Y., Hu, X., Fu, Z., Zhao, Y., He, H., Lu, Y.: Multifunctional hybrid metasurfaces for dynamic tuning of terahertz waves. Adv Opt Mater **6**(14), 1800257 (2018)
32. Shu, F.Z., Yu, F.F., Peng, R.W., Zhu, Y.Y., Xiong, B., Fan, R.H., Wang, Z.H., Liu, Y., Wang, M.: Dynamic plasmonic color generation based on phase transition of vanadium dioxide. Adv Opt Mater **6**(7), 1700939 (2018)
33. Shu, F.Z., Wang, J.N., Peng, R.W., Xiong, B., Fan, R.H., Gao, Y.J., Liu, Y., Qi, D.X., Wang, M.: Electrically driven tunable broadband polarization states via active metasurfaces based on Joule-heat-induced phase transition of vanadium dioxide. Laser Photonics Rev **15**(10), 2100155 (2021)
34. Pitchappa, P., Kumar, A., Singh, R., Lee, C., Wang, N.: Terahertz MEMS metadevices. J Micromech Microeng **31**(11), 113001 (2021)
35. Huang, Y., Okatani, T., Inomata, N., Kanamori, Y.: A reconfigurable ladder-shaped THz metamaterial integrated with a microelectromechanical cantilever array. Appl Phys Lett **122**(5), 051705 (2023)
36. Fu, Y., Xu, X., Lin, Y.S.: Actively programmable MEMS-based racetrack-shaped terahertz metamaterial. J Appl Phys **131**(11), 115301 (2022)
37. Silalahi, H.M., Chiang, W.F., Shih, Y.H., Wei, W.Y., Su, J.Y., Huang, C.Y.: Folding metamaterials with extremely strong electromagnetic resonance. Photon Res **10**(9), 2215–2222 (2022)
38. Shih, K., Pitchappa, P., Manjappa, M., Ho, C.P., Singh, R., Yang, B., Singh, N., Lee, C.: Active MEMS metamaterials for THz bandwidth control. Appl Phys Lett **110**(16), 161108 (2017)
39. Kan, T., Isozaki, A., Kanda, N., Nemoto, N., Konishi, K., Takahashi, H., Kuwata-Gonokami, M., Matsumoto, K., Shimoyama, I.: Enantiomeric switching of chiral metamaterial for terahertz polarization modulation employing vertically deformable MEMS spirals. Nat Commun **6**(1), 8422 (2015)
40. Fan, K., Padilla, W.J.: Dynamic electromagnetic metamaterials. Mater Today **18**(1), 39–50 (2015)
41. Liu, M., Susli, M., Silva, D., Putrino, G., Kala, H., Fan, S., Cole, M., Faraone, L., Wallace, V.P., Padilla, W.J., Powell, D.A., Shadrivov, I.V., Martyniuk, M.: Ultrathin tunable terahertz absorber based on MEMS-driven metamaterial. Microsyst Nanoeng **3**(1), 17033 (2017)
42. Zheludev, N.I., Plum, E.: Reconfigurable nanomechanical photonic metamaterials. Nat Nanotechnol **11**(1), 16–22 (2016)
43. Kan, T., Isozaki, A., Kanda, N., Nemoto, N., Konishi, K., Kuwata-Gonokami, M., Matsumoto, K., Shimoyama, I.: Spiral metamaterial for active tuning of optical activity. Appl Phys Lett **102**(22), 221906 (2013)
44. Zhao, X., Schalch, J., Zhang, J., Seren, H.R., Duan, G., Averitt, R.D., Zhang, X.: Electromechanically tunable metasurface transmission waveplate at terahertz frequencies. Optica **5**(3), 303–310 (2018)
45. Först, M., Manzoni, C., Kaiser, S., Tomioka, Y., Tokura, Y., Merlin, R., Cavalleri, A.: Nonlinear phononics as an ultrafast route to lattice control. Nat Phys **7**(11), 854–856 (2011)
46. Fleischer, S., Zhou, Y., Field, R., Nelson, K.: Molecular orientation and alignment by intense single-cycle THz pulses. Phys Rev Lett **10**(16), 163603 (2011)
47. Kong, D., Wu, X., Wang, B., Nie, T., Xiao, M., Pandey, C., Gao, Y., Wen, L., Zhao, W., Ruan, C., Miao, J., Li, Y., Wang, L.: Broadband spintronic terahertz emitter with magnetic-field manipulated polarizations. Adv Opt Mater **7**(20), 1900487 (2019)
48. Wu, W., Lendinez, S., Kaffash, M.T., Schaller, R.D., Wen, H., Jungfleisch, M.B.: Controlling polarization of spintronic THz emitter by remanent magnetization texture. Appl Phys Lett **121**(5), 052401 (2022)
49. Agarwal, P., Huang, L., Ter Lim, S., Singh, R.: Electric-field control of nonlinear THz spintronic emitters. Nat Commun **13**(1), 4072 (2022)
50. Federici, J., Moeller, L.: Review of terahertz and subterahertz wireless communications. J Appl Phys **107**(11), 111101 (2010)
51. Kim, T.T., Oh, S.S., Kim, H.D., Park, H.S., Hess, O., Min, B., Zhang, S.: Electrical access to critical coupling of circularly polarized waves in graphene chiral metamaterials. Sci Adv **3**(9), e1701377 (2017)
52. Qi, T., Shin, Y.H., Yeh, K.L., Nelson, K.A., Rappe, A.M.: Collective coherent control: synchronization of polarization in ferroelectric $PbTiO_3$ by shaped THz fields. Phys Rev Lett **102**(24), 247603 (2009)
53. Tinoco, I. Jr, Cantor, C.R.: Application of optical rotatory dispersion and circular dichroism to the study of biopolymers. In: Methods of Biochemical Analysis. (1970)
54. Song, Z., Zhang, L., Liu, Q.H.: High-efficiency broadband cross polarization converter for near-infrared light based on anisotropic plasmonic meta-surfaces. Plasmonics **11**(1), 61–64 (2016)
55. Zhang, B., Lv, L., He, T., Chen, T., Zang, M., Zhong, L., Wang, X., Shen, J., Hou, Y.: Active terahertz device based on optically controlled organometal halide perovskite. Appl Phys Lett **107**(9), 093301 (2015)
56. Guo, J., Kim, J.Y., Yang, S., Xu, J., Choi, Y.C., Stein, A., Murray, C.B., Kotov, N.A., Kagan, C.R.: Broadband circular polarizers via coupling in 3D plasmonic meta-atom arrays. ACS Photonics **8**(5), 1286–1292 (2021)

57. Liu, Z., Du, H., Li, J., Lu, L., Li, Z.Y., Fang, N.X.: Nano-kirigami with giant optical chirality. Sci Adv **4**(7), eaat4436 (2018)
58. Wang, Z., Jing, L., Yao, K., Yang, Y., Zheng, B., Soukoulis, C.M., Chen, H., Liu, Y.: Origami-based reconfigurable metamaterials for tunable chirality. Adv Mater Adv Mater **29**(27), 1700412 (2017)
59. Landau J., Kearsley L.P., Pitaevskii E.M., Lifshitz J.B.: Sykes: Electrodynamics of Continuous Media (1984)
60. McConney, M.E., Kulkarni, D.D., Jiang, H., Bunning, T.J., Tsukruk, V.V.: A new twist on scanning thermal microscopy. Nano Lett **12**(3), 1218–1223 (2012)
61. Zheng, L.S., Lu, M.S.C.: A large-displacement CMOS micromachined thermal actuator with comb electrodes for capacitive sensing. Sens Actuators A Phys. **136**(2), 697–703 (2007)
62. King, T.G., Preston, M.E., Murphy, B.J.M., Cannell, D.S.: Piezoelectric ceramic actuators: a review of machinery applications. Precis Eng **12**(3), 131–136 (1990)
63. Wu, C., Kahn, M., Moy, W.: Piezoelectric ceramics with functional gradients: a new application in material design. J Am Ceram Soc **79**(3), 809–812 (1996)
64. Makino, E., Mineta, T., Mitsunaga, T., Kawashima, T., Shibata, T.: Sphincter actuator fabricated with PDMS/SMA bimorph cantilevers. Microelectron Eng **88**(8), 2662–2665s (2011)
65. Krulevitch, P., Lee, A.P., Ramsey, P.B., Trevino, J.C., Hamilton, J., Northrup, M.A.: Thin film shape memory alloy microactuators. J Microelectromech Syst **5**(4), 270–282 (1996)
66. Cavalleri, A., Tóth, C., Siders, C.W., Squier, J.A., Ráksi, F., Forget, P., Kieffer, J.C.: Femtosecond structural dynamics in VO_2 during an ultrafast solid-solid phase transition. Phys Rev Lett **87**(23), 237401 (2001)
67. Wang, X., Dong, K., Choe, H.S., Liu, H., Lou, S., Tom, K.B., Bechtel, H.A., You, Z., Wu, J., Yao, J.: Multifunctional microelectro-opto-mechanical platform based on phase-transition materials. Nano Lett **18**(3), 1637–1643 (2018)
68. Liu, K., Cheng, C., Cheng, Z., Wang, K., Ramesh, R., Wu, J.: Giant-amplitude, high-work density microactuators with phase transition activated nanolayer bimorphs. Nano Lett **12**(12), 6302–6308 (2012)
69. Nikishkov, G.P.: Curvature estimation for multilayer hinged structures with initial strains. J Appl Phys **94**(8), 5333–5336 (2003)
70. Sepúlveda, N., Rúa, A., Cabrera, R., Fernández, F.: Young's modulus of VO_2 thin films as a function of temperature including insulator-to-metal transition regime. Appl Phys Lett **92**(19), 191913 (2008)
71. Merle, B.: Mechanical Properties of Thin Films Studied by Bulge Testing (2013)
72. Guo, X.G., Zhou, Z.F., Sun, C., Li, W.H., Huang, Q.A.: A simple extraction method of young's modulus for multilayer films in MEMS applications. Micromachines **8**(7), 201 (2017)
73. Kanda, N., Konishi, K., Kuwata-Gonokami, M.: Terahertz wave polarization rotation with double layered metal grating of complimentary chiral patterns. Opt Express **15**(18), 11117–11125 (2017)

Zhixiang Huang is currently a Ph.D. candidate in the Department of Materials Science and Engineering at the University of Delaware, USA. Zhixiang Huang received a M.S. degree in Materials Engineering from the University of Southern California, USA in 2018 and a B.S. degree in Chemistry from Sun Yat-sen University, China in 2016. Zhixiang Huang's research interests include phase-transition materials, nanophotonics, and nanomaterials.

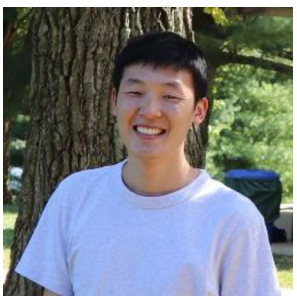

Weipeng Wu earned his bachelor's degree in 2013 from Wuhan University, China and is currently pursuing his doctoral degree in the Department of Physics and Astronomy at the University of Delaware, USA. In 2022, he received the Daicar-Bata Award for his outstanding research paper from the Department of Physics and Astronomy. Additionally, in 2023, he was honored with a Doctoral Fellowship for Excellence by the university's graduate college.

At the heart of Weipeng's research endeavors lies a keen interest in time-domain/resolved terahertz (THz) spectroscopy. His work focuses on leveraging this innovative technique to characterize ultrafast spin dynamics, understand and control the integration of different material classes that enables the transduction of THz frequency excitations across interfaces, thereby granting control over emergent THz functionality.

Eric Herrmann received his B.S. degree in Physics from West Chester University of Pennsylvania, USA in 2018 and is currently a Ph.D. candidate in the Department of Materials Science and Engineering at the University of Delaware, USA. His research interests include nanophotonics and strain engineering of two-dimensional materials.

Ke Ma is currently a Ph.D. candidate in the Department of Materials Science and Engineering at the University of Delaware, USA. Ke Ma received a B.S. degree in Chemistry from Tsinghua University, China in 2019. Ke Ma's research interests include nanophotonics, 2D materials, and tunable optical devices.

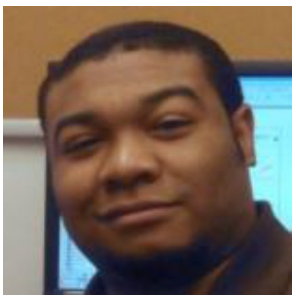

Zizwe Chase is a former Bridge-to-Faculty scholar at University of Illinois at Chicago and a former Postdoctoral Fellow in the SAMPL group of the Physics Department of Howard University, USA. He received his B.S. degree in Chemistry from Morehouse College, B.S. degree in Chemical Engineering from Georgia Institute of Technology, and Ph.D. in Chemical Engineering from Washington State University, USA. His research interests include topics in chemistry and physics namely interfacial interactions at catalytic surfaces and light matter interactions with 2D metamaterials. He is interested in using various spectroscopic techniques to probe interfacial regions and nanomaterials. He is a former Goddard Space Flight Center and Pacific Northwest National Lab intern.

Thomas A. Searles is an Assoc. Prof. at University of Illinois Chicago (UIC), USA. He received his B.S. degree from Morehouse College and his Ph.D. degree in Applied Physics from Rice University, USA. Prior to UIC, he was a Martin Luther King Visiting Professor at MIT and served as the Director of the IBM-HBCU Quantum Center at Howard University, USA. Thomas's research focuses on a variety of topics in quantum engineering with applications in quantum computing, photonics and communications.

M. Benjamin Jungfleisch is an Associate Professor of Physics and Astronomy at the University of Delaware, USA. His research interests encompass many magnetism-related effects, including spin-transport phenomena and magnetization dynamics in nanostructures. He received the Department of Energy Early Career Research Award, the National Science Foundation EPSCoR RII Track-4 Fellowship, and the National Science Foundation CAREER Award. Before joining the University of Delaware, he was a postdoctoral researcher at Argonne National Laboratory. He received his M.S. and Ph.D. degrees in Physics from the University of Kaiserslautern, Germany.

Xi Wang is currently an assistant professor in the Department of Materials Science and Engineering at the University of Delaware (UD), USA. Dr. Xi Wang received his Ph.D. degree in Electrical Engineering from the State University of New York at Buffalo, USA in 2014 and a B.S. degree in Microelectronics from Tsinghua University, China in 2007. Dr. Xi Wang was a postdoctoral scholar at the University of California, Berkeley, USA before he started his appointment at UD in 2018. Dr. Xi Wang's research focuses on the area of nanophotonics, nanomaterials, and tunable nanophotonic devices.